DETERMINING PARAMETERS FOR ANATOMICAL LANDMARKS OF THE HUMERUS FROM POINT CLOUDS ACQUIRED FROM THE BONE'S SURFACE

U. von Jan*, D. Sandkühler**, L. Kirsch***, O. Rühmann*** and H.M. Overhoff**

* Institute of Medical Informatics, Hannover Medical School, Hannover, Germany
** Medical Engineering Laboratory, University of Applied Sciences Gelsenkirchen, Gelsenkirchen, Germany
*** Orthopedic Department, Hannover Medical School, Hannover, Germany

jan.ute.von@mh-hannover.de

Abstract: The definition of reproducible geometric measures is important for navigated, medical image based implantations of the humeral part of a shoulder endoprosthesis which aims at finding the anatomic optimal position of the prosthesis. Boileau et. al. [1, 2] recommend the use of certain bony landmarks for a prosthesis alignment to the humerus. In a pilot study, we investigated whether the specified landmarks can be reliably calculated based on the segmentation results obtained from freehand acquired 3-D ultrasound image volumes of the humerus. Methods for the identification of these landmarks and their accuracy are described.

Introduction

During the implantation of a prosthesis into the humerus, surgeons often tend to reconstruct the preoperative anatomical relations. A typical problem with older prosthesis models was that they only offered restricted possibilities to realize all demanded relations between e.g. proximal humerus shaft axis, retrotorsion angle, and humeral head orientation. Modern 3^{rd} and 4^{th} generation prostheses for the humerus allow the adjustment of the prosthesis according to these parameters in a flexible manner. The opportunity of a precise reconstruction on the one hand makes it necessary to accurately determine the preoperative anatomical situation on the other hand.

The definition of a reproducible local coordinate system (LCS) is a first necessity for an objective quantification of anatomical relations in bones. For the shoulder joint, the ISB recommends the use of the center of the humeral head and the medial and lateral epicondyles [3]. For a precise and accurately navigated implantation of a humerus endoprosthesis, even these landmarks are not sufficient. Boileau et. al. [1, 2] recommend the use of certain additional bony landmarks (fig. 1) like the proximal humeral shaft for the objective description of the shoulder joint's geometry.

For a completely ultrasound image based navigated implantation these landmarks must be determined from ultrasound images. The presentablity of all landmarks in 3-D ultrasound volumes has already been shown [4]. Furthermore, a semi-automatic detection of the landmarks in such image volumes was already presented [5]. In this work, we describe a method for the identification of the spatial location of landmarks. Additionally, the derivation of more abstract anatomical measures from such landmarks is presented.

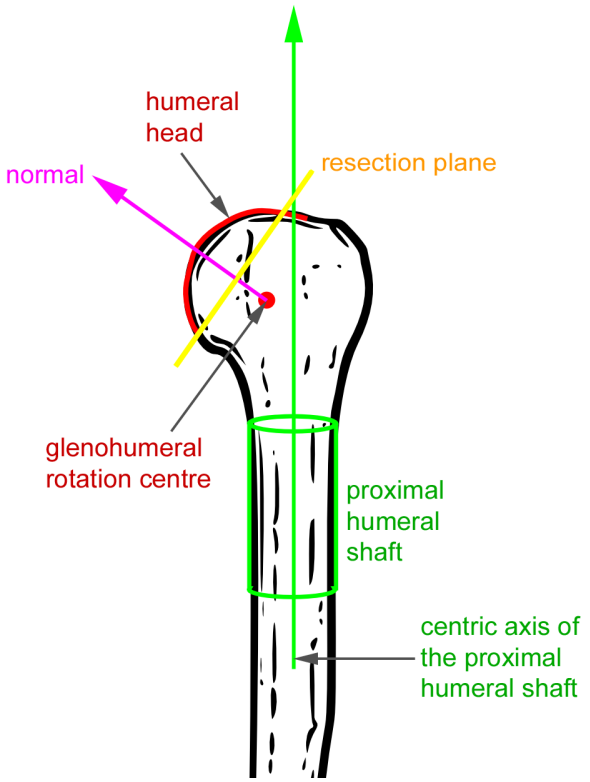

Figure 1: Humerus landmarks.

ISSN: 1727-1983

Materials and Methods

The geometry of ten human humeri was determined by scanning the entire humeral surface with 3-D ultrasound to determine specific anatomical landmarks. The acquisition technique, the landmark measurement and the parameter identification are described in the following.

Technical equipment

An appropriate image acquisition technique, using a conventional 2-D ultrasound imaging system (Nemio^{TM} SSA-550A, Toshiba, Tokyo, Japan) employing B-mode imaging from 6-12 MHz and an infrared optical localizer system (Polaris^{TM}, Northern Digital Inc., Waterloo, Ontario, Canada) was specified and developed (fig. 3).

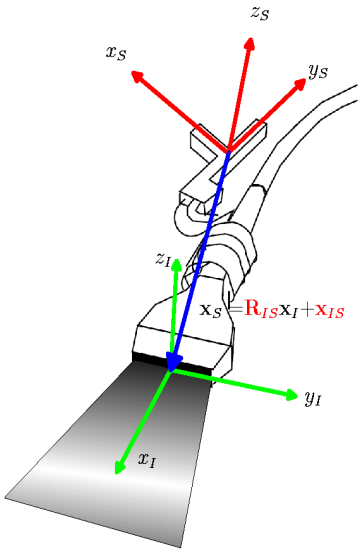

Figure 2: Ultrasound probe with optical DRB and rigid transformation; Figure modified from [6].

An infrared optical dynamic reference base (DRB) was attached to the ultrasound probe. The position as well as the orientation of the DRB and the 2-D images were recorded simultaneously during a manually performed freehand sweep on a standard PC (Intel Pentium^{TM} IV, 3.2 GHz, 512MB). The B-mode images were captured from the S-VHS video output of the ultrasound imaging system and digitized using a conventional external video grabbing card (ADVC^{TM} 55, Canopus, San Jose, California, USA). The image series consisted of approx. 1000-1500 B-mode images at a sample rate of 6 images/sec.

Calibration of the transducer

A 3-D ultrasound image volume is generated from 2-D B-mode images. For this the position and orientation of the images must by known. These pose data cannot be measured directly using a conventional transducer, so an infrared position sensor is attached to the probe. To finally determine the transducer's pose data, the measured sensor's pose data must be transformed using the coordinate system transformation from the DRB position sensor to the B-mode ultrasound image (fig. 4).

Calibration – method

This coordinate system transformation must be determined from a calibration. The experimental data come from a perspex cube, whose surface is recorded in freehand ultrasound sweeps. As an ultrasound image can be assumed to be a half plane, the intersection between a B-mode image and a cube's plane is a straight line (see fig. 5). These image data are utilized to determine the unknown parameters of the coordinate system transformation parameters [7], i.e. three rotation angles and three translation components, thus the image points can be arranged to form a cube's plane.

Calibration – parameter identification

To identify the unknown parameters, the following transformation equations are used, which relate the reference (localizer, R), DRB position sensor (S), and ultrasound image (I) coordinate systems. In the transformations from localizer R to sensor S

$$\mathbf{x}_R = \hat{\mathbf{R}}_{SR}\mathbf{x}_S + \hat{\mathbf{x}}_{SR} \tag{1}$$

and from sensor S to B-mode image I

$$\mathbf{x}_S = \mathbf{R}_{IS}\mathbf{x}_I + \mathbf{x}_{IS}, \tag{2}$$

$\mathbf{R}_{OR}$ denotes a 3×3 matrix that represents the rotation from a reference coordinate system R to an object coordinate system O, and $\mathbf{x}_{OR}$ denotes the respective 3×1 translation vector.

The coordinate system transformation from localizer R to sensor S is known from measurements ($\hat{\mathbf{R}}_{SR}$, $\hat{\mathbf{x}}_{SR}$). Furthermore all cube's surface points $\mathbf{x}_R$, apart from measurement errors e, lie on a plane:

$$\mathbf{x}_R^T \cdot \mathbf{n} - \rho = e \approx 0, \tag{3}$$

where $\mathbf{n}$ denotes the plane's normal vector with $|\mathbf{n}| = 1$, and ρ is the shortest distance between the reference coordinates system's origin and the (infinite) plane.

The cube's surface points are visualized as a straight line in the ultrasound images. They can be determined – e.g. by a Hough transform [8] where the correct line (fig. 5) can be determined correctly as the maximum of the accumulator (fig. 6) even for noisy image data – and have image coordinates $\mathbf{x}_I$. To calculate their corresponding positions in the reference coordinate system, eq. (2) is inserted into eq. (1):

$$\begin{aligned}\mathbf{x}_R &= \hat{\mathbf{R}}_{SR}\left(\mathbf{R}_{IS}\mathbf{x}_I + \mathbf{x}_{IS}\right) + \hat{\mathbf{x}}_{SR} \\ &= \hat{\mathbf{R}}_{SR}\mathbf{R}_{IS}\mathbf{x}_I + \hat{\mathbf{R}}_{SR}\mathbf{x}_{IS} + \hat{\mathbf{x}}_{SR}\end{aligned} \tag{4}$$

The substitution of eq. (4) in the plane equation (3)

$$\left(\hat{\mathbf{R}}_{SR}\mathbf{R}_{IS}\mathbf{x}_I + \hat{\mathbf{R}}_{SR}\mathbf{x}_{IS} + \hat{\mathbf{x}}_{SR}\right)^T \cdot \mathbf{n} - \rho = e \approx 0 \tag{5}$$

ISSN: 1727-1983

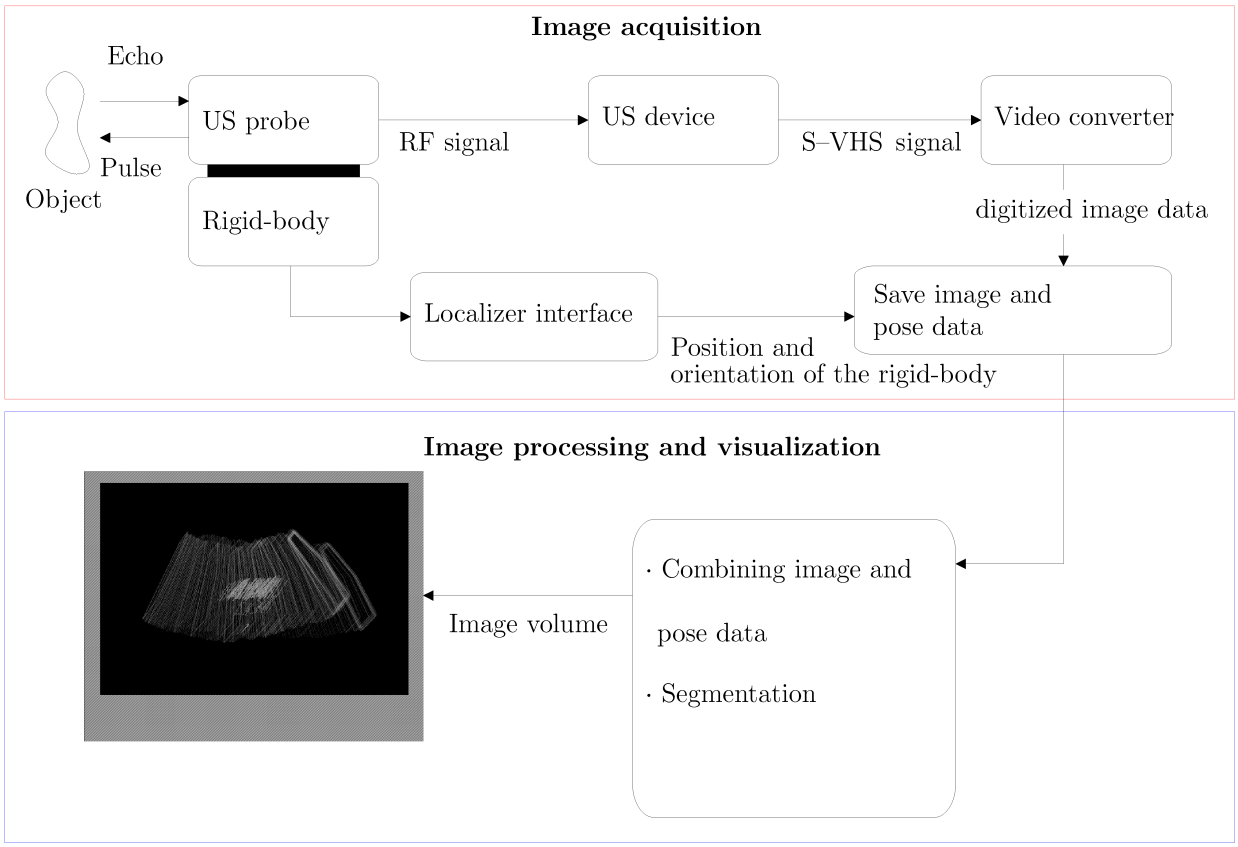

Figure 3: Recording of three-dimensional ultrasound image volumes: technical realization.

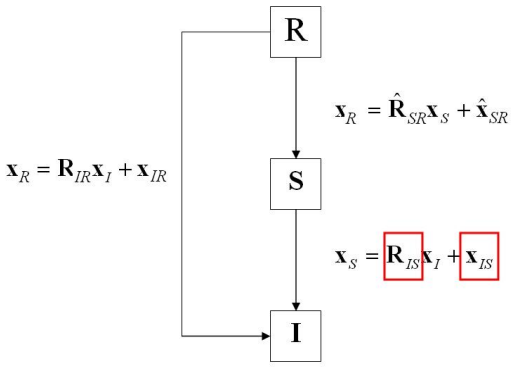

Figure 4: Coordinate system transformations between the objects: R = reference (localizer), S = DRB position sensor, and I = ultrasound image. $\mathbf{R}_{IS}$ and $\mathbf{x}_{IS}$ must be identified from a calibration.

leads to an equation for the determination of the six unknown parameters. For this, three additional unknown parameters were introduced by the plane equation (3), therefore nine parameters need to be identified.

In this setup, three orthogonal cube planes are used. For each plane, $N \approx 15$ images are recorded. The image vector

$$\mathbf{x}_I(i,j) = \begin{bmatrix} x_{I_x}(i,j) \cdot s_x \\ x_{I_y}(i,j) \cdot s_y \\ 0 \end{bmatrix}$$

shall now denote the j-th pixel on the line in the i-th image, $i = 1, 2, 3, \ldots, N-1, N$. s_x denotes the width and s_y the height of a pixel in millimeters.

To reduce the computational effort of the parameter identification, only two ($j = 1,2$) representative pixels of the i-th image are exploited, e.g. those pixels which are furthest apart from each other. Eq. (5) is thereby changed as follows:

$$\begin{aligned}&[\hat{\mathbf{R}}_{SR}(i)\ \mathbf{R}_{IS}\ \mathbf{x}_I(i,j) + \\ &\hat{\mathbf{R}}_{SR}(i)\ \mathbf{x}_{IS} + \hat{\mathbf{x}}_{SR}(i)]^T \cdot \mathbf{n} - \rho = e(i,j)\end{aligned} \tag{6}$$

where

$$\begin{aligned} i &= 1,2,3,\ldots,N-1,N, \\ j &= 1,2. \end{aligned}$$

$J(\mathbf{R}_{IS}, \mathbf{x}_{IS}, \mathbf{n})$ is the error function for $2N$ points, which has to be minimized:

$$\begin{aligned} J(\mathbf{R}_{IS}, \mathbf{x}_{IS}, \mathbf{n}) &= \sum_{i=1}^{N}\sum_{j=1}^{2}[(\hat{\mathbf{R}}_{SR}(i)\,(\mathbf{R}_{IS}\mathbf{x}_I(i,j) + \mathbf{x}_{IS}) \\ &\quad + \hat{\mathbf{x}}_{SR}(i) - \bar{\mathbf{x}}_R)^T \cdot \mathbf{n}]^2 \rightarrow min. \end{aligned} \tag{7}$$

ISSN: 1727-1983

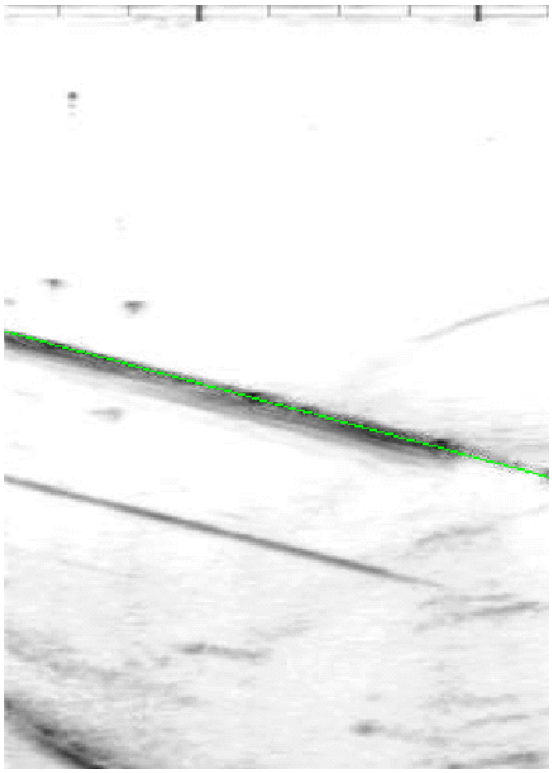

Figure 5: B-mode ultrasound image (gray scale inverted) containing a straight line (green) which belongs to a cube's plane. Below, an additional line artefact is visible.

The distance ρ to the plane is then given by the center point $\bar{\mathbf{x}}_R$:

$$\rho = \bar{\mathbf{x}}_R^T \cdot \mathbf{n} \quad \text{with } \bar{\mathbf{x}}_R = \frac{1}{N}\sum_{i=1}^{N} \mathbf{x}_R. \tag{8}$$

The eight free parameters in eq. (7) cannot be calculated in closed form. They are identified using a numerical optimization algorithm. Here, the simplex method according to Nelder and Mead is applied [9].

After the parameters are determined, the coordinate system transformation from DRB sensor S to B-mode image I (2) is known. Now the spatial position $\mathbf{x}_R$ can be calculated for each image pixel $\mathbf{x}_I$ using eq. (4).

Approximation of anatomical structures by geometric bodies

As known from anatomy, the humeral head only forms a segment of a sphere whose area is only about 40% of the whole spherical surface. Accordingly only 80% - 90% of the proximal humeral shaft data fit to a cylinder. This introduces an inherent instability for the identification of the parameters of geometric bodies since the points additionally are in general substantially corrupted by segmentation errors. To generate a robust, i.e. data insensitive identification, an iterative approach is used for the spherical fit [10]. The robustification consists

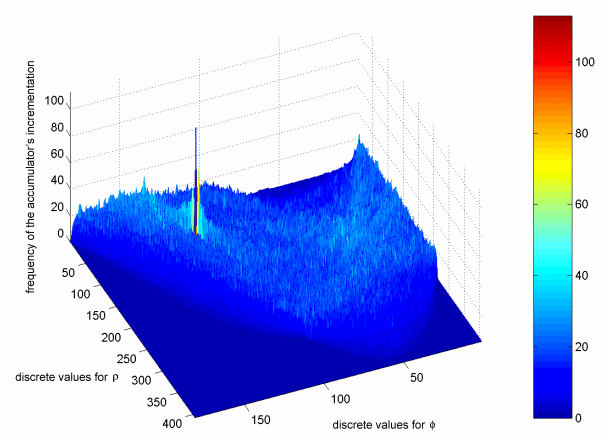

Figure 6: Hough accumulator with unique maximum indicating the parameters for a straight line.

in the iterative computation of reference bodies and the stepwise rejection of irrelevant voxels. Such procedures tend to be numerically costly dependent on their algorithmic structure. Typically, an iteration is used to systematically reject false data until the approximation is "optimal" in a certain sense. The approximation itself should be determined straightforward to reduce processing time.

A segmentation procedure shall have generated scattered data from a previously recorded 3-D ultrasound image volume that now shall be approximated by a cylinder (humerus shaft) and by a sphere (humerus head) respectively in each case.

Approximation – humerus shaft

N humeral shaft voxels $\mathbf{x}_R(i)$, $1 \le i \le N$, determined by a specific segmentation algorithm, shall be approximated by a cylinder with center $\mathbf{x}_0 = [x_0\ y_0\ z_0]^T$, symmetry axis vector $\mathbf{x}_c$, and radius R. These parameters are determined by an iterative algorithm.

This algorithm is initialized by a principal components analysis (PCA, [11, chap. 4.5]) of the voxels. Their center point is a starting guess for $\mathbf{x}_0$, and the PCA axis belonging to the largest eigenvalue gives the initial value for $\mathbf{x}_c$.

The following algorithm is processed:

(0) determine initial values $\mathbf{x}_0$ and $\mathbf{x}_c$ from PCA
(1) determine all radii r_i between voxels $\mathbf{x}_R(i)$ and cylinder axis $\mathbf{x}_c$:

$$r_i = \frac{|\mathbf{x}_c \times (\mathbf{x}_R(i) - \mathbf{x}_0)|}{|\mathbf{x}_0|}$$

(2) sort all determined radii r_i and store them in a distance vector $\mathbf{r}$
(3) determine the cylinder radius R as the median of the distance vector $\mathbf{r}$: $R = median(\mathbf{r})$
(4) determine the radius errors

$$e_i = median(\mathbf{r}) - r_i \tag{9}$$

ISSN: 1727-1983

(5) compute the sum of squares $J = \sum_i e_i^2$, where i is in the range of 5% - 95% of the distance vector $\mathbf{r}$ to reject invalid measurements
(6) if the minimization criterion of the numerical optimization algorithm [9] is fulfilled go to step 7, else generate new parameters $\mathbf{x}_0$ and $\mathbf{x}_c$ and go to step 1.
(7) $\mathbf{x}_0$, $\mathbf{x}_c$ and R are the optimal cylinder parameters, J is is a measure for the accuracy of the fit

Approximation – humerus head

N humeral head voxels $\mathbf{x}_R(i) = [x_{Ri}\ y_{Ri}\ z_{Ri}]^T$, $1 \leq i \leq N$ may have been generated by another specific segmentation procedure. They form a set of scattered data, which shall be approximated by a sphere (10) with center $[x_0\ y_0\ z_0]^T$ and radius R:

$$R^2 = (x_{Ri} - x_0)^2 + (y_{Ri} - y_0)^2 + (z_{Ri} - z_0)^2, \quad 1 \leq i \leq N. \tag{10}$$

At first glance, the sphere's parameter identification seems to be a non-linear problem. By re-ordering of the sphere equation (10), it is transformed to the parameter-linear form

$$\underbrace{[-2x_{Ri}\ -2y_{Ri}\ -2z_{Ri}\ 1]}_{\mathbf{a}_i^T} \cdot \underbrace{\left[x_0\ y_0\ z_0\ \left(-R^2 + x_0^2 + y_0^2 + z_0^2\right)\right]^T}_{\boldsymbol{\theta}} = \underbrace{-x_{Ri}{}^2 - y_{Ri}{}^2 - z_{Ri}{}^2}_{b_i}. \tag{11}$$

Applied to all N humeral head voxels, these equations can be noted in a compact vector form

$$\mathbf{A}\boldsymbol{\theta} = \begin{bmatrix} \mathbf{a}_1^T \\ \mathbf{a}_2^T \\ \vdots \\ \mathbf{a}_N^T \end{bmatrix} \boldsymbol{\theta}, \qquad \mathbf{b} = \begin{bmatrix} b_1 \\ b_2 \\ \vdots \\ b_N \end{bmatrix}.$$

Due to segmentation and measurement errors, eq. (11) can only be solved up to an approximation error e_i if it is applied to $N > 4$ humeral head voxels:

$$\mathbf{a}_i^T \cdot \boldsymbol{\theta} - \mathbf{b}_i = e_i \approx 0. \tag{12}$$

Thus, for all voxels, an overdetermined linear equation system

$$\mathbf{A}\boldsymbol{\theta} - \mathbf{b} = \mathbf{e} \approx \mathbf{0} \tag{13}$$

must be solved.

This system shall be determined to minimize the sum of squared errors (minimal least squares fit): $\mathbf{e}^T\mathbf{e} \rightarrow min$. This minimum is found for the parameter vector [11, chap. 19.2]

$$\boldsymbol{\theta} = \left(\mathbf{A}^T\mathbf{A}\right)^{-1}\mathbf{A}^T\mathbf{b}. \tag{14}$$

$\left(\mathbf{A}^T\mathbf{A}\right)^{-1}\mathbf{A}^T$ is the so called pseudoinverse of the matrix $\mathbf{A}$. Eq. (14) can be calculated efficiently, whereas the robustification strategy – see step (0) of the following algorithm – greatly influences the processing time.

The approximation humerus head approximation has the following algorithmic structure:

(0) randomly reject 10% of the segmented voxels
(1) determine the sphere parameters $\boldsymbol{\theta}$ from eq. (14)
(2) compute the sum of squares $J = \mathbf{e}^T\mathbf{e}$ with $\mathbf{e}$ from eq. (13)
(3) if the minimization criterion of the numerical optimization algorithm [9] is fulfilled go to step (4), else go to step (0).
(4) calculate the optimal sphere parameters from $\boldsymbol{\theta}$, J is is a measure for the accuracy of the fit

Results

Fig. 7 depicts typical calibration results. The calibration of the B-mode ultrasound images generated a mean plane approximation error (eq. 5) of less than 3 pixels or 0.3 *mm*. About 80% of the pixels fit better than 5 pixels or 0.5 *mm*. The transformation of voxel positions to the reference coordinate system is therefore very precise.

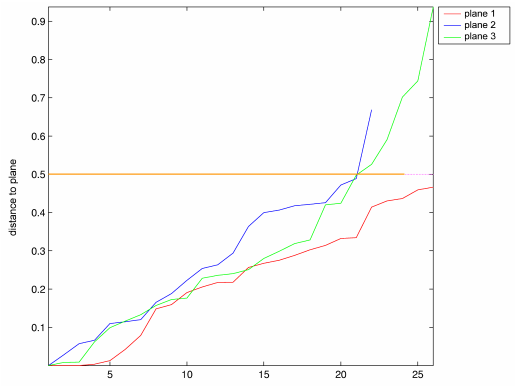

Figure 7: Deviation $|e(i,j)|$ from approximated planes

The humeral head and shaft can be approximated by geometrical bodies using the described algorithms. The 90% quantile of the absolute approximation errors is less than 2 *mm*. Results of the approximation are shown in fig. 8.

As depicted in fig. 9, the distance between the bone's surface and the idealized geometry varies mostly between 0 *mm* and approx. 2 *mm* with only a few outliers, which confirms the assumption that approximation of the proximal part of the humerus by a cylinder and of the humeral head by a sphere is meaningful.

Discussion

The determination of humerus landmarks is successful. The approach to approximate geometric bodies using data-robust algorithms must be further investigated for its sensitivity to the portion of rejected data. Additionally, the segmentation algorithm has to be refined to reduce

ISSN: 1727-1983

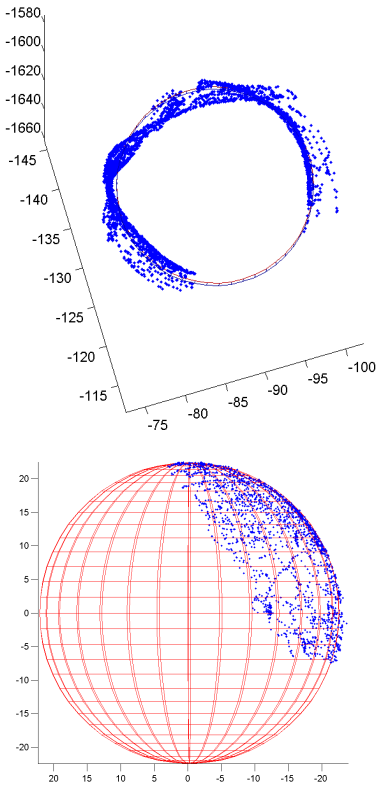

Figure 8: Approximation error $|e_i|$ data vs. cylinder (top view, cf. eq. (9)) and data vs. sphere (side view, cf. eq. (12)).

or better to avoid falsely segmented pixels. To be able to implement a complete planning scenario, an automatic detection of the epicondyles must be realized.

The geometric modeling of anatomical structures seems to be applicable also e.g. for the lower limb, especially the femoral head, neck and proximal shaft.

Conclusions

The chosen approach for landmark identification in the humerus can be assumed to be valid due to the good visual and numeric approximation of the segmented data.

Acknowledgment

We thank the German Research Foundation for the funding of this project in the DFG-SPP 1124 program.

References

[1] P. BOILEAU and G. WALCH. The tree-dimensional geometry of the proximal humerus - implications for surgical technique and prosthetic design. *J Bone Joint Surg Br*, 79:857–865, 1997.

[2] P. BOILEAU and G. WALCH. A new concept in shoulder arthroplasty. *J Shoulder Elbow Surg*, 8(5):443–451, 1999.

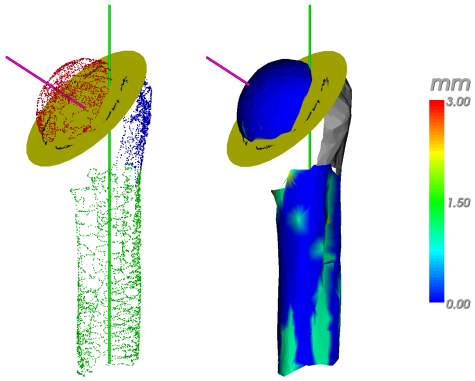

Figure 9: Sampled data points and reconstructed surface (colored according to distance to the sphere resp. cylinder).

[3] G. WU, F.C.T. VAN DER HELM, H.E.J. VEEGER, M. MAKHSOUS, P. VAN ROY, C. ANGLING, J. NAGELS, A.R. KARDUNAI, K. MCQUADE, X. WANG, F.W. WERNER, and B. BUCHHOLZ. ISB recommendation on definitions of joint coordinate systems of various joints for the reporting of human joint motion – part II: shoulder, elbow, wrist and hand. *Journal of Biomechanics*, 38:981–992, 2005.

[4] D. SANDKÜHLER, L. KIRSCH, and H.M. OVERHOFF. Presentability of anatomical structures of the shoulder joint in 3-d ultrasound image volumes. In *Biomedizinische Technik*, volume 49, pages 878–9. Schiele & Schön, 2004.

[5] U. VON JAN, D. SANDKÜHLER, L. KIRSCH, H.M. OVERHOFF, and O. RÜHMANN. Ultrasound volume based surgical planning for prosthesis implantation in the shoulder joint. In H.P. Meinzer, H. Handels, A. Horsch, and T. Tolxdorff, editors, *Bildverarbeitung für die Medizin 2005*, pages 435–439, Berlin, Heidelberg, New York, 2005. Springer.

[6] R.N. ROHLING. *3D Freehand Ultrasound: Reonstruction and Spatial Compounding*. PhD thesis, Churchill College, 1998.

[7] J. WITTENBURG. *Dynamics of Systems of Rigid Bodies*. B.G. Teubner, Stuttgart, 1977.

[8] R. O. DUDA and P. E. HART. Use of the hough transformation to detect lines and curves in pictures. *Comm. ACM*, 15:11–5, 1972.

[9] J. A. NELDER and R. MEAD. A simplex method for function minimization. *Computer Journal*, 7:308–13, 1965.

[10] H.M. OVERHOFF, S. EHRICH, and U. VON JAN. Reliable identification of sphere-shaped femoral heads in 3-d image data. In Kenneth M. Henson, editor, *Medical Imaging 1999: Image Processing*, volume 3661 of *Procs SPIE*, pages 1377–1387, 1999.

[11] I.N. BRONSHTEIN, K.A. SEMENDYAYEV, G. MUSIOL, and H. MUEHLIG. *Handbook of Mathematics*. Spinger, Berlin, Heidelberg, New York, 4th edition, 2004.

ISSN: 1727-1983